Buildings & Industrial Energy Systems
Energy Technologies Area
Lawrence Berkeley National Laboratory

Technical assessment of the negative solar radiative forcing and atmospheric cooling benefits of surface brightening projects

Ronnen Levinson[1], Pouya Vahmani[1], Frank Klink[2], Hashem Akbari[3]

[1]Lawrence Berkeley National Laboratory, [2]Climate Resolve, [3]Concordia University

Energy Technologies Area
September 2026

This work was supported by the Assistant Secretary Office of Critical Minerals and Energy Innovation (CMEI) of the US Department of Energy
under Contract No. DE-AC02-05CH11231.

7th International Conference on Countermeasures to Urban Heat Islands (IC2UHI), pp. 1–10. ©2026, Nanjing, China. (PREPRINT)

Technical assessment of the negative solar radiative forcing and atmospheric cooling benefits of surface brightening projects

Ronnen Levinson[1], Pouya Vahmani[2], Frank Klink[3], Hashem Akbari[4]
[1,2]*Lawrence Berkeley National Laboratory, Berkeley, California, USA*
[3]*Climate Resolve, Los Angeles, California, USA*
[4]*Concordia University, Montreal, Quebec, CAN*

ABSTRACT

Brightening the Earth's surface can increase the outflux of sunlight to space. This diminishes the net (downward minus upward) solar flux into the Earth's radiative system, providing negative solar radiative forcing that can cool the atmosphere. We are quantifying the extent to which surface-brightening projects, such as installing solar-reflective roofs and pavements, can raise bottom-of-atmosphere (BOA) albedo, increase top-of-atmosphere (TOA) solar outflux, and reduce regional and global atmospheric temperatures. We compared four approaches to assessing BOA albedo: roof- or pavement-product documentation; local measurements with an albedometer (back-to-back pyranometers); extrapolation from extended-color aerial images (blue, green, red, and near-infrared); and multispectral satellite images sharpened by convolution with aerial images, selecting the last. We developed a technique to calculate the atmosphere's upward solar transmittance anywhere in the Earth's tropical and temperate zones based on analysis of BOA irradiances reported in the National Solar Radiation Database, then computed radiative forcing factors relating the increase in TOA solar outflux (negative solar radiative forcing) to the rise in BOA albedo (surface brightening). We identified atmospheric modeling experiments using both regional and global circulation models to quantify the atmospheric cooling potential of reflective surfaces at regional and global scales. These activities provide regional estimates of the atmospheric cooling benefits of reflective roofs and pavements.

Keywords: cool surface, negative solar radiative forcing, atmospheric cooling, remote sensing

Introduction

Brightening the Earth's surface can increase the outflux of sunlight to space. This diminishes the net (downward minus upward) solar flux into the Earth system, providing negative solar radiative forcing that can cool the atmosphere. The Technical Working Group (TWG) of the Shine On Initiative is quantifying how surface-brightening projects, such as installing solar-reflective roofs and pavements, can raise bottom-of-atmosphere (BOA) albedo, increase top-of-atmosphere (TOA) solar outflux, and reduce regional and global atmospheric temperatures. This manuscript describes our development of evaluation, measurement, and verification (EMV) tools to assess increases in BOA albedo and TOA outflux induced by real projects, and our atmospheric modeling (AM) efforts to quantify the cooling and CO_2 equivalency achieved by simulated surface-brightening campaigns.

[1] RML27@cornell.edu, ORCID: 0000-0003-1463-1359
[2] PVahmani@LBL.gov, ORCID: 0000-0003-2519-6671
[3] FrankWKlink@gmail.com, ORCID: 0000-0003-2224-7402
[4] Hashem@HashemAkbari.com, ORCID: 0000-0001-8808-8112

Assessing albedo rise

We seek to quantify the increase in BOA albedo from reflective roofs, pavements, and other brightened surfaces, to verify the successful execution of cool-surface projects, and to estimate the associated negative solar radiative forcing and atmospheric cooling benefits. BOA albedo can be obtained from documentation, such as the initial and aged solar reflectance values provided by the roof and wall product rating programs of the Cool Roof Rating Council (Cool Roof Rating Council, n.d.); by local measurement, such as mounting an albedometer (back-to-back pyranometers) over a roof or pavement (ASTM International, 2021); or via remote sensing with aerial or satellite imagery that spans enough of the solar spectrum to estimate albedo.

Albedo-rise scenarios, such as those attainable from making all low-sloped roofs white and all steep roofs cool-colored, can be generated from published values of roof or pavement solar reflectance; however, this approach is less applicable to a specific project unless both the existing and new surfaces have been rated and labeled. In-situ reflectance measurements with an albedometer are highly accurate but can be difficult to scale because they require specialized equipment, a trained operator, and safe access to the roof or pavement for characterization. Remote sensing of roof albedo using submeter resolution, extended-color images (blue, green, red, and near-infrared) collected by aerial surveys, such as the National Agriculture Imagery Program (NAIP) in the USA, was first demonstrated for seven major California cities (Ban-Weiss et al., 2015) and later combined with Sentinel-2 satellite imagery and machine learning to generate an urban albedo dataset spanning 34 major U.S. cities (Yi et al., 2025). This technique is promising but would require other NAIP-like imagery to extend outside the USA. A parallel effort by the World Resources Institute (WRI) and Google has sharpened Sentinel-2's low-resolution (10 – 20 m) hyperspectral images (blue, green, red, near-infrared, short-wave IR1, and short-wave IR2) by convolving them with decimeter-resolution extended-color imagery to generate sub-meter urban albedo rasters (Fork et al., 2026). Lawrence Berkeley National Laboratory researchers used an early version of such rasters to estimate potential roof and pavement albedo increases in Los Angeles County (Robinson et al., 2024).

We plan to use the WRI-Google albedo data to assess roof and pavement albedos once these datasets are publicly released, tentatively in 2026. We are also developing a "Flying Albedometer", a small drone carrying a lightweight payload, including an albedometer, a datalogger, a video camera, an inclinometer, a GPS receiver, a height-above-surface sensor, and a wireless bridge, to measure roof and pavement reflectance. This device could characterize individual projects or calibrate and validate remotely sensed albedo rasters, such as those generated by WRI and Google.

Estimating negative solar radiative forcing

Raising BOA albedo R_{BOA} by ΔR_{BOA} will increase TOA solar upflux (upwelling solar radiance) J_{TOA} by

$$\Delta J_{\mathrm{TOA}} = k_{\mathrm{SF}}\, \Delta R_{\mathrm{BOA}} \tag{1}$$

where the solar forcing factor

$$k_{\mathrm{SF}} = I_{\mathrm{BOA}}\, T_{\mathrm{up}} \tag{2}$$

is the product of BOA solar downflux (downwelling solar radiance) I_{BOA} and the upward (BOA to TOA) solar atmospheric transmittance T_{up}. We want to relate T_{up} to the more readily obtainable downward (TOA to BOA) solar atmospheric transmittance

$$T_{\text{down}} = I_{\text{BOA}}/I_0 \quad (3)$$

where I_{BOA} is the global horizontal solar irradiance (GHSI) at BOA and I_0 is the extraterrestrial horizontal solar irradiance at TOA. The downward solar atmospheric transmittance for a beam at solar zenith angle z is

$$T_{\text{down}}(z) = \frac{\int_{\text{sol}} i_0(z,x)\, t(z,x) dx}{\int_{\text{sol}} i_0(z,x)\, dx} \quad (4)$$

where $i_0(z,x)$ is the extraterrestrial horizontal solar spectral irradiance at wavelength x, $t(z,x)$ is the atmosphere's spectral transmittance, and each integration is performed over the solar spectrum. The corresponding upward solar atmospheric transmittance is

$$T_{\text{up}}(z) = \frac{\int_{\text{sol}} i_0(z,x)\, t(z,x)^2\, r(z,x)\, dx}{\int_{\text{sol}} i_0(z,x)\, t(z,x)\, r(z,x)\, dx} \quad (5)$$

where $r(z,x)$ is the spectral reflectance of the surface at BOA, assumed horizontal. Spectral transmittance $t(z,x)$ along a specific path is the same upward and downward by Helmholtz reciprocity (Clarke & Parry, 1985).

If BOA reflectance does not vary with wavelength (i.e., the surface is spectrally "gray"), Eq. (5) simplifies to

$$T_{\text{up}}(z) = \frac{\int_{\text{sol}} i_0(z,x)\, t(z,x)^2\ dx}{\int_{\text{sol}} i_0(z,x)\, t(z,x)\ dx} \quad (6)$$

and $T_{\text{up}}(z) \geq T_{\text{down}}(z)$ by the Cauchy–Schwarz inequality for integrals (Ford, 2015). The physical explanation is that the atmosphere has already extinguished solar flux at wavelengths where $t(x)$ is low in downward transmission (TOA to BOA). However, if BOA reflectance varies with wavelength, reflectance $r(z,x)$ could be anti-correlated to transmittance $t(z,x)$ (one high where the other is low), yielding $T_{\text{up}}(z) < T_{\text{down}}(z)$. We compared T_{up} to T_{down} for roof-reflected sunlight by (a) using the Simple Model of the Atmospheric Radiative Transfer of Sunshine (SMARTS) 2.9.5 (Gueymard, n.d.) to model solar spectral irradiances $i_0(x)$ and $i_{\text{BOA}}(x)$ at air mass 2 (AM2; $z = 60°$) for the clear-sky conditions underlying the ASTM G173 reference air mass 1.5 spectra (National Lab of the Rockies, n.d.); (b) calculating solar spectral transmittance $t(x) = i_{\text{BOA}}(x)/i_0(x)$; and (c) applying the solar spectral reflectances $r(x)$ for 190 roofing products measured in a prior LBNL study (Ban-Weiss et al., 2015) when computing T_{up}. There were no obvious signs of anti-correlation between $r(x)$ and $t(x)$, and we found that upward solar transmittance was approximately 10-14% greater than downward solar transmittance at air mass 2 (Figure 1). Hence, we will assume that $T_{\text{up}}(z) \geq T_{\text{down}}(z)$.

We approximate the BOA surface as a horizontal, perfectly diffuse reflector. Since a beam of light reflected at an angle of 60° from the surface normal will travel the same path length as perfectly diffused light reflected from the same surface (Kubelka, 1948), the upward solar atmospheric transmittance of light reflected from this surface

$$T_{\text{up,diffuse}} = \frac{1}{90°} \int_0^{90°} T_{\text{up}}(z)\, dz \geq \frac{1}{90°} \int_0^{90°} T_{\text{down}}(z)\, dz \quad (7)$$

should equal or exceed $T_{\text{down,AM2}} = T_{\text{down}}(z = 60°)$. Therefore

$$k'_{\text{SF}} = I_{\text{BOA}}\, T_{\text{down,AM2}} \quad (8)$$

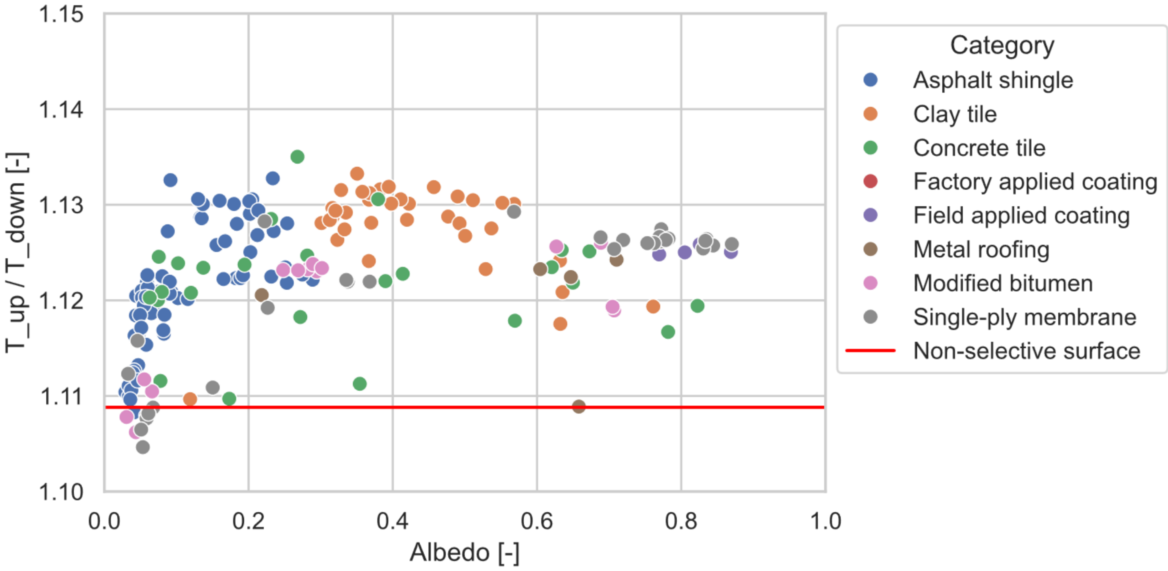

Figure 1. AM2 atmospheric solar transmittance ratio (up/down) vs. roof albedo, by type of roofing.

is a lower bound to the solar forcing factor k_{SF}.

The National Solar Radiation Database (NSRDB) maintained by the National Laboratory of the Rockies provides satellite-derived, sub-hourly modeled values of solar irradiance at spatial resolutions of 2–4 km and temporal resolutions of 10–15 min for the USA & Americas (2018-present); Asia, Australia, & Pacific (2016-2020); and Europe, Africa, & Asia (2017-2019) (NLR Developer Network, n.d.). We downloaded year-2019 sub-hourly values of GHSI I_{BOA}, clear-sky GHSI $I_{\mathrm{BOA,clear}}$, and aerosol optical depth τ (among other fields) for 1,000 well-separated tropical cities and 978 well-separated temperate cities, each with a population of at least 100,000; used the pvlib Python toolbox to calculate contemporaneous values of I_0; and then analyzed each city as follows.

We (a) interpolated $I_{\mathrm{BOA}}(z)$, $I_{\mathrm{BOA,clear}}(z)$, $I_0(z)$, and $\tau(z)$ for integer values of z in the morning (z decreasing) and afternoon (z increasing) of each day; (b) calculated $T_{\mathrm{down}}(z) = I_{\mathrm{BOA}}(z)/I_0(z)$ and sky clarity $c_{\mathrm{sky}}(z) = I_{\mathrm{BOA}}(z)/I_{\mathrm{BOA,clear}}(z)$; and (c) regressed a linear fit (form $y = a\,x + b$) of $T_{\mathrm{down}}(z)$ to $c_{\mathrm{sky}}(z)$ when the sky was cloudy ($c_{\mathrm{sky}} < 1$) and an exponential decay fit (form $y = a\,e^{-b\,x} + c$) of $T_{\mathrm{down}}(z)$ to $\tau(z)$ when the sky was clear ($c_{\mathrm{sky}} = 1$). We then computed

$$T_{\mathrm{down,diffuse,cloudy}}(c_{\mathrm{sky}}) = \frac{1}{90°}\int_0^{90°} T_{\mathrm{down,cloudy}}(z, c_{\mathrm{sky}})\,dz \tag{9}$$

$$T_{\mathrm{down,diffuse,clear}}(\tau) = \frac{1}{90°}\int_0^{90°} T_{\mathrm{down,clear}}(z, \tau)\,dz \tag{10}$$

in each tropical city (since the sun reaches zenith at least once a year in the tropics) and

$$T_{\mathrm{down,AM2,cloudy}}(c_{\mathrm{sky}}) = T_{\mathrm{down,cloudy}}(c_{\mathrm{sky}}, \mathrm{z} = 60°) \tag{11}$$

$$T_{\mathrm{down,AM2,clear}}(\tau) = T_{\mathrm{down,clear}}(\tau, \mathrm{z} = 60°) \tag{12}$$

in every tropical and temperate city (since the sun reaches a zenith angle of 60° at least once a year in the tropical and temperate latitudes). Using Honolulu, HI (latitude 21.3°N) as the test case, we confirmed that the diffuse and AM2 values of $T_{\mathrm{down,cloudy}}$ matched to within 1%, and

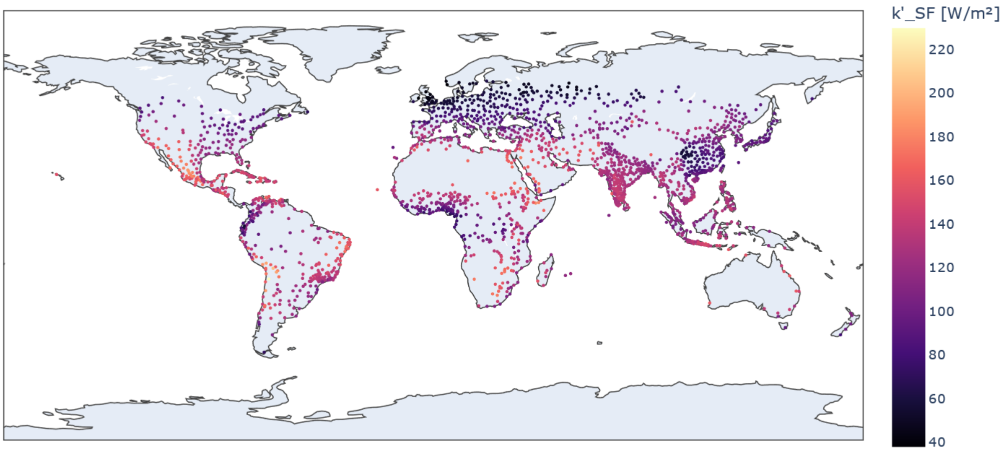

(a)

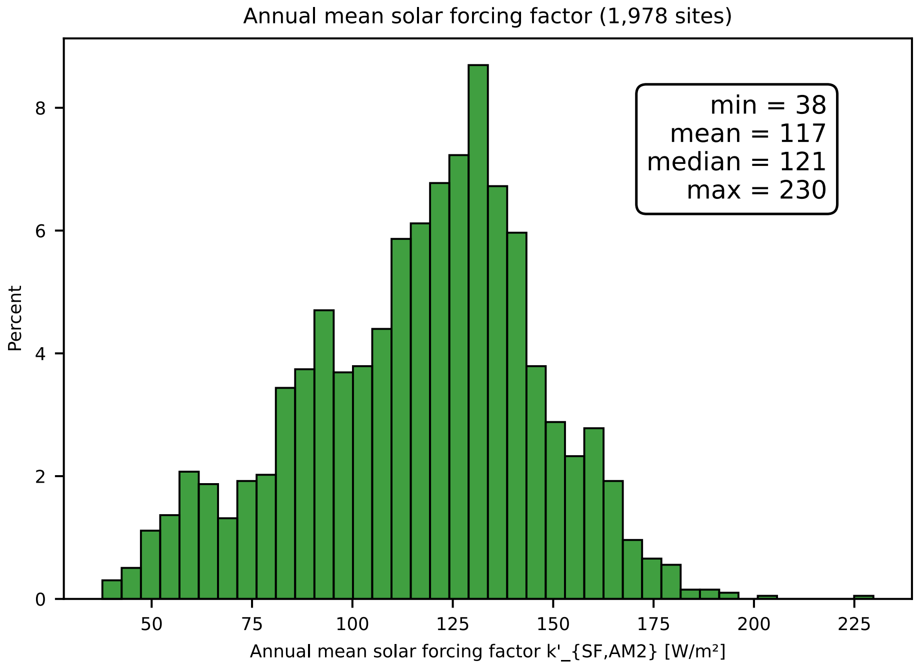

(b)

Figure 2. Map (a) and histogram (b) of the annual mean value of $k'_{\mathrm{SF,AM2}}$, the lower bound to the solar forcing factor k_{SF}, in 1,978 cities around the world.

that the diffuse and AM2 values of $T_{\mathrm{down,clear}}$ also agreed to within 1%. Finally, we computed in each tropical and temperate city (a) sub-hourly values of $T_{\mathrm{down,AM2}} = T_{\mathrm{down,AM2,cloudy}}(c_{\mathrm{sky}})$ if $c_{\mathrm{sky}} < 1$ or $T_{\mathrm{down,AM2,clear}}(\tau)$ if $c_{\mathrm{sky}} = 1$; (b) sub-hourly values of $k'_{\mathrm{SF}} = I_{\mathrm{BOA}}\, T_{\mathrm{down,AM2}}$; and (c) the annual mean value of k'_{SF}. Items (b) and (c) are lower bounds to the corresponding values of k_{SF} that would be obtained using $T_{\mathrm{up}} \geq T_{\mathrm{down,AM2}}$.

The annual mean value of k'_{SF} across the 1,978 cities ranged from 38 to 230 W/m², with mean 117 W/m² and median 121 W/m² (Figure 2). Using this median value as an example, raising BOA albedo by 0.50 would increase outgoing solar flux at TOA by at least 0.50 × 121 W/m² = 61 W/m².

Atmospheric modeling framework

To complement the radiative-forcing estimates derived from irradiance and atmospheric transmittance, we use regional climate modeling (RCM) to quantify the atmospheric cooling produced by prescribed surface-albedo increases. These cooling estimates, together with the radiative-forcing calculations, support forcing-based and temperature-response-based CO_2-

Table 1. Albedo values used in baseline and reflective-surface cases

	Low-slope roof	Steep roof	Wall	Road
Baseline	0.2	0.2	0.3	0.1
Reflective Surface	0.8	0.4	0.8	0.3

equivalency assessments. Our scalable, region-at-a-time RCM workflow begins with North America and will extend across major world regions, while planned global climate modeling (GCM) experiments will provide a global benchmark.

Prior studies show that reflective surfaces can produce spatially varied temperature responses through meteorological feedbacks (Millstein & Menon, 2011; Vahmani et al., 2019; Vahmani & Jones, 2017), while fine-resolution modeling and observations in Los Angeles demonstrate neighborhood-scale effects of albedo and vegetation (Taha et al., 2018; Vahmani & Ban-Weiss, 2016). Our RCM framework extends beyond individual cities and subcontinental case studies by applying standardized regional domains sequentially to build globally comparable coverage. The simulations use the Weather Research and Forecasting model (WRF), the Building Effect Parameterization (BEP) urban canopy model (Hendricks et al., 2020; Martilli et al., 2002), and a Local Climate Zone (LCZ)-based urban representation (Stewart & Oke, 2012). The initial North America experiment spans 2025 with hourly output to resolve diurnal, seasonal, and extreme-heat responses.

North America regional modeling results

The North America RCM domain covers the contiguous United States (CONUS) and portions of Mexico and Canada. The Control scenario uses baseline urban-surface albedos, while Total Adoption applies reflective roofs, walls, and pavements at 100% adoption. Figure 3 presents the annual-mean 2-m air-temperature response (panel a), ranked results for 38 metropolitan areas (panel b), and cooling efficacy normalized by the imposed surface-albedo increase (panel c). Four partial cool-roof adoption scenarios were also simulated but are not discussed here.

The 12-km configuration resolves regional meteorological gradients and metropolitan-scale variability, while the BEP urban canopy framework and LCZ-based representation provide a standardized description of urban form. Albedo changes are prescribed for roofs, walls, and roads, with values summarized in Table 1. Baseline roof and road albedos follow previous studies (Alleman & Heitzman, 2019; Robinson et al., 2024), while city-to-city differences are represented by LCZ-based urban morphology and surface fractions.

The year-2025 North America RCM results show that Total Adoption reduces the annual-mean 2-m air temperature in all evaluated metropolitan areas (Figure 3b). Across metros, the mean metro-mean annual temperature reduction is 0.2 °C, and the largest metro-mean annual reduction is 0.4 °C. Cooling is substantially stronger in summer than in winter: the CONUS-mean urban temperature reduction is 0.3 °C in summer compared with 0.1 °C in winter. The weaker winter cooling may nevertheless be undesirable in heating-dominated periods because it can increase building heating demand. Cooling efficacy varies substantially across metros when normalized by the imposed albedo increase (Figure 3c), ranging from 0.014 to 0.07 °C per 0.01 increase in surface albedo; this spread reflects local differences in insolation, urban fraction, and land–atmosphere energy-balance feedbacks. Overall, the predominance of cooling indicates that the direct radiative effect of increased surface reflectance generally exceeds compensating meteorological feedbacks in the annual-mean city-scale response. The results shown here represent the first full-year realization (2025) of the North America regional domain. Because interannual variability in circulation, clouds, and moisture can modulate the

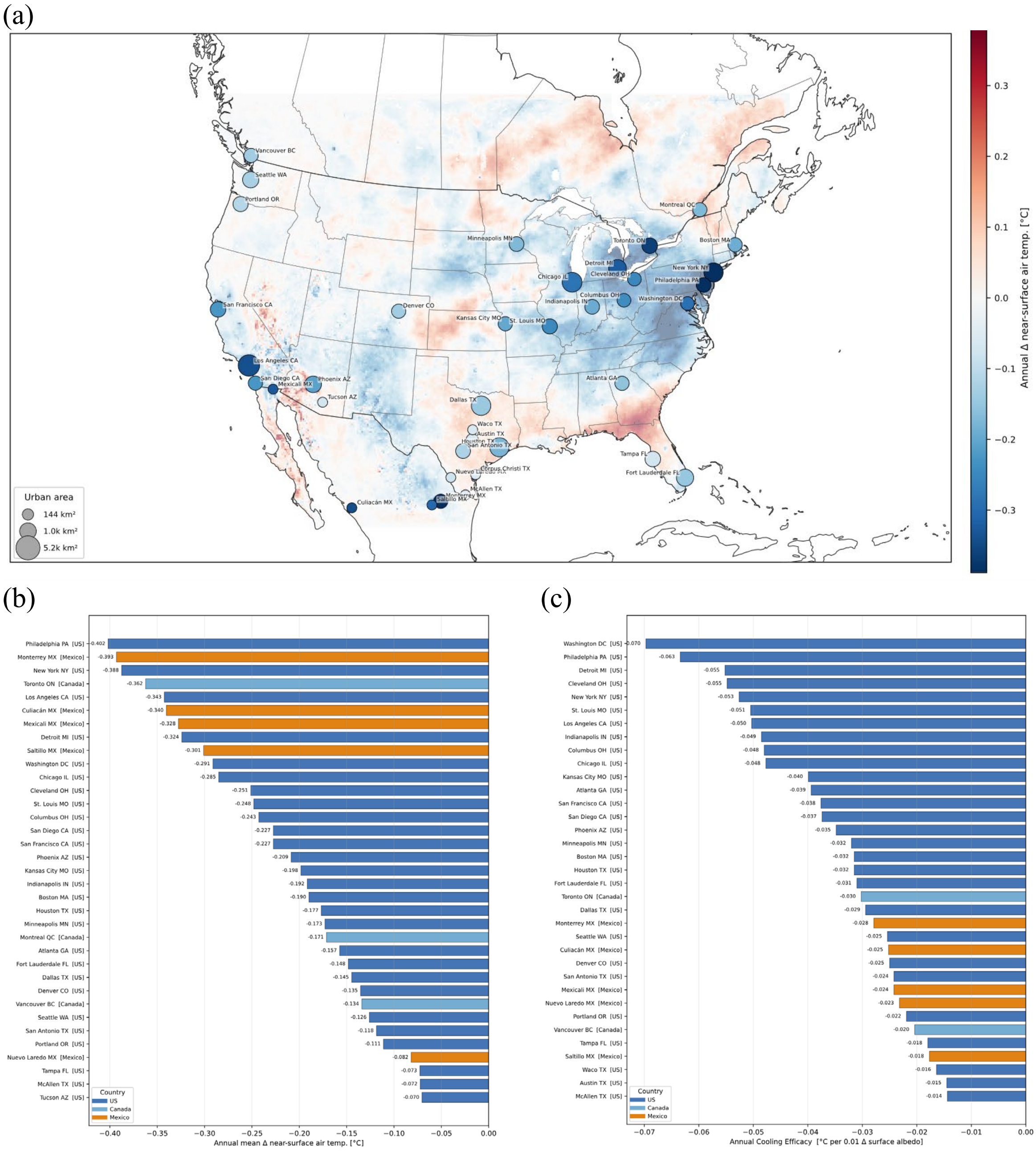

Figure 3. North America WRF experiments (2025): Total Adoption − Control. (a) Annual-mean change in 2-m air temperature (T2), reported as ΔT2 (°C), over CONUS with 38 metropolitan-area summaries (bubble color = metro-mean ΔT2; bubble size = urban area). (b) Ranked metro-mean annual ΔT2 for 38 metropolitan areas (urban-pixel means; WRF grid cells with urban fraction > 0.1). (c) Ranked metro cooling efficacy, defined as urban-pixel-mean ΔT2 per 0.01 increase in surface albedo (ΔALBEDO) between Total Adoption and Control.

realized air-temperature response to albedo perturbations, we plan additional simulation years to strengthen the robustness of the estimated cooling signal before extending the workflow to the next region.

CO_2-equivalency

CO_2 offsets from surface brightening are commonly estimated using two related equivalency concepts. Radiative-forcing-based equivalency compares the negative forcing from albedo increase to the positive forcing from atmospheric CO_2; using this framing, Akbari et al. (2009) estimated that increasing the albedo of 1 m² of surface area by 0.01 is comparable to reducing CO_2 output by about 2.5 kg. Temperature-response-based equivalency instead maps the longer-term temperature response from sustained albedo increases to the temperature response that would result from CO_2 reductions; Akbari et al. (2012) used climate simulations to compare these responses and reported an offset of about 7 kg CO_2 per 0.01 increase in surface albedo per 1 m². As Akbari (2026) emphasized, early estimates were largely global averages and did not resolve strong regional dependence arising from spatial variability in solar irradiance and cloudiness. In this paper, we begin linking both radiative-forcing estimates (from irradiance and transmittance) and modeled atmospheric cooling signals to CO_2-equivalent offsets.

As an initial temperature-response-based CO_2-equivalent estimate from the North America regional experiment (distinct from the RF-based approach described above), we apply a first-order, area-weighted scaling that relates the domain-mean annual cooling signal to an Earth-mean equivalent temperature response. Let the domain-mean annual 2-m air temperature difference be

$$T_{\mathrm{D}} = T_{2,\mathrm{Total\ Adoption}} - T_{2,\mathrm{Control}} \quad (13)$$

where T_2 is 2-m air temperature. The corresponding Earth-mean temperature response is

$$T_{\mathrm{G}} = T_{\mathrm{D}} \frac{A_{\mathrm{D}}}{A_{\mathrm{G}}} \quad (14)$$

where A_{D} is the CONUS land area over which T_{D} is averaged and A_{G} is Earth's surface area. For the year-2025 North America simulation, the annual-mean all-land temperature response across CONUS is $T_{\mathrm{D}} = -0.020$ °C. Using $A_{\mathrm{D}} = 1.24 \times 10^{13}$ m^2 and $A_{\mathrm{G}} = 5.10 \times 10^{14}$ m^2, this yields $T_{\mathrm{G}} = -4.9 \times 10^{-4}$ °C. To express cooling per unit modified area and albedo increase, we define

$$\lambda_{\alpha} = \frac{-T_{\mathrm{G}}}{A_{\mathrm{M}}\, \Delta\alpha} \quad (15)$$

where λ_{α} is the global cooling-response coefficient per unit modified area and albedo increase, defined here as a positive magnitude; $A_{\mathrm{M}} = 9.35 \times 10^{10}$ m^2 (649 urban grid cells at 12 km × 12 km) and $\Delta\alpha = 0.04936$. Using the Akbari et al. (2012) temperature–CO_2 relationship (0.01 °C $\leftrightarrow$ 21 Gt CO_2) yields an implied offset of 2.2 kg CO_2 per 0.01 increase in surface albedo per 1 m², and 1.02 Gt CO_2 when applied to the full modified area in the Total Adoption case. This scaling is a first-order estimate and does not account for the spatial structure of forcing or efficacy. Because this estimate is based on a single simulation year and an area-weighted scaling, it should be interpreted as preliminary; additional RCM years are planned to improve robustness before extending the same calculation to other regions.

In future work, radiative-forcing-based CO_2-equivalent offsets will be computed by converting prescribed albedo increases to negative solar radiative forcing using the irradiance and transmittance framework developed earlier and applying the regional formulation described by Akbari (2026). Planned GCM experiments will be used to estimate global mean temperature responses to prescribed albedo perturbations and to benchmark the regional-model-derived scaling and CO_2-equivalent offsets across standardized regions.

Summary

We plan to use high-resolution urban albedo data to be released by Google to estimate the albedos of roofs and pavements before and after they are brightened. We will also build and test a drone-mounted "Flying Albedometer" to measure the before-and-after albedos of individual cool-surface projects and to calibrate and validate remotely sensed urban albedo datasets. Meanwhile, we have already developed and tested a method that uses sub-hourly BOA irradiance values from the NSRDB to estimate the annual mean solar forcing factor (the ratio of the TOA solar upflux increase to the BOA albedo rise) for virtually any city in the world.

Building on these EMV and radiative-forcing methods, we are developing a complementary atmospheric modeling framework to translate project-scale albedo changes into regional cooling and CO_2-equivalent offsets. Using WRF with a multi-layer urban canopy representation, the regional implementation over North America indicates that the strongest reflective-surface adoption scenario yields a mean city-mean annual 2-m air temperature reduction of 0.2 °C, with largest city-mean annual reduction of 0.4 °C, in the initial 2025 simulation year. We will extend the simulations to additional years to strengthen robustness to interannual variability and then apply the same region-at-a-time workflow to other major world regions. Finally, we will link modeled negative solar radiative forcing and atmospheric cooling to CO_2-equivalent offsets using both forcing-based and temperature-response–based approaches, including regionally resolved formulations that account for geographic variability in solar irradiance and atmospheric transmittance. For the initial North America temperature-response estimate, this yields about 2.2 kg CO_2 offset per 0.01 increase in surface albedo per 1 m^2, equivalent to about 1.02 Gt CO_2 for the Total Adoption case.

Acknowledgements

This study was funded by the ClimateWorks Foundation and supported by the Office of Critical Minerals and Energy Innovation (CMEI) of the U.S. Department of Energy under Contract No. DE-AC02-05CH11231.

References

Akbari, H. (2026). A simplified method to calculate atmospheric CO2 equivalency for changing surface albedo. *Urban Climate*, *65*, 102795. https://doi.org/10.1016/j.uclim.2026.102795

Akbari, H., Matthews, H. D., & Seto, D. (2012). The long-term effect of increasing the albedo of urban areas. *Environmental Research Letters*, *7*(2), 024004. https://doi.org/10.1088/1748-9326/7/2/024004

Akbari, H., Menon, S., & Rosenfeld, A. (2009). Global cooling: Increasing world-wide urban albedos to offset CO2. *Climatic Change*, *94*(3–4), 275–286. https://doi.org/10.1007/s10584-008-9515-9

Alleman, J., & Heitzman, M. (2019). *Quantifying Pavement Albedo: Final Report* [NCAT Report 19-09]. National Center for Asphalt Technology. https://rosap.ntl.bts.gov/view/dot/62003

ASTM International. (2021). *ASTM E1918-21: Standard Test Method for Measuring Solar Reflectance of Horizontal and Low-Sloped Surfaces in the Field*. ASTM International. https://doi.org/10.1520/E1918-21

Ban-Weiss, G. A., Woods, J., & Levinson, R. (2015). Using remote sensing to quantify albedo of roofs in seven California cities, Part 1: Methods. *Solar Energy*, *115*, 777–790. https://doi.org/10.1016/j.solener.2014.10.022

Clarke, F. J. J., & Parry, D. J. (1985). Helmholtz Reciprocity: Its validity and application to reflectometry. *Lighting Research & Technology*, *17*(1), 1–11. https://doi.org/10.1177/14771535850170010301

Cool Roof Rating Council. (n.d.). *Roof Rating Program*. Retrieved February 2, 2026, from https://coolroofs.org/programs/roof-rating-program

Ford, W. (2015). Orthogonal Vectors and Matrices. In *Numerical Linear Algebra with Applications* (pp. 103–118). Elsevier. https://doi.org/10.1016/B978-0-12-394435-1.00006-5

Fork, D., Wesley, E. J., Banerjee, S., Batchu, V., Chennapragada, A., Crossan, K., Cronkite-Ratcliff, B., Delich, E., Goulden, T., Kansal, M., Kemp, J., Mackres, E., Mayer, Y., Milman, R., Platt, J. C., Prabhakara, S., Prasad, G., Shetty, S., Stanton, C., … Hutyra, L. R. (2026). Estimating high-resolution albedo for urban applications. *Nature Communications*, *17*(1), 4815. https://doi.org/10.1038/s41467-026-73436-y

Gueymard, C. (n.d.). *SMARTS: Simple Model of the Atmospheric Radiative Transfer of Sunshine*. Retrieved July 12, 2026, from https://www.nlr.gov/grid/solar-resource/smarts

Hendricks, E. A., Knievel, J. C., & Wang, Y. (2020). Addition of Multilayer Urban Canopy Models to a Nonlocal Planetary Boundary Layer Parameterization and Evaluation Using Ideal and Real Cases. *Journal of Applied Meteorology and Climatology*, *59*(8), 1369–1392. https://doi.org/10.1175/JAMC-D-19-0142.1

Kubelka, P. (1948). New Contributions to the Optics of Intensely Light-Scattering Materials. Part I. *JOSA*, *38*(5), 448–457. https://doi.org/10.1364/JOSA.38.000448

Martilli, A., Clappier, A., & Rotach, M. W. (2002). An Urban Surface Exchange Parameterisation for Mesoscale Models. *Boundary-Layer Meteorology*, *104*(2), 261–304. https://doi.org/10.1023/A:1016099921195

Millstein, D., & Menon, S. (2011). Regional climate consequences of large-scale cool roof and photovoltaic array deployment. *Environmental Research Letters*, *6*(3), 034001. https://doi.org/10.1088/1748-9326/6/3/034001

National Lab of the Rockies. (n.d.). *Reference Air Mass 1.5 Spectra*. Retrieved February 1, 2026, from https://www.nrel.gov/grid/solar-resource/spectra-am1.5

NLR Developer Network. (n.d.). *NSRDB Data Downloads*. Retrieved February 2, 2026, from https://developer.nrel.gov/docs/solar/nsrdb/

Robinson, A., Fernandes, S., Hong, T., Lee, S. H., Levinson, R., & Piette, M. A. (2024). *Potential Urban Heat Island Countermeasures and Building Energy Efficiency Improvements in Los Angeles County*. Lawrence Berkeley National Laboratory. https://doi.org/10.20357/B7M30K

Stewart, I. D., & Oke, T. R. (2012). Local Climate Zones for Urban Temperature Studies. *Bulletin of the American Meteorological Society*, *93*(12), 1879–1900. https://doi.org/10.1175/BAMS-D-11-00019.1

Taha, H., Levinson, R., Mohegh, A., Gilbert, H., Ban-Weiss, G., & Chen, S. (2018). Air-Temperature Response to Neighborhood-Scale Variations in Albedo and Canopy Cover in the Real World: Fine-Resolution Meteorological Modeling and Mobile Temperature Observations in the Los Angeles Climate Archipelago. *Climate*, *6*(2), 53. https://doi.org/10.3390/cli6020053

Vahmani, P., & Ban-Weiss, G. A. (2016). Impact of remotely sensed albedo and vegetation fraction on simulation of urban climate in WRF-urban canopy model: A case study of the urban heat island in Los Angeles. *Journal of Geophysical Research: Atmospheres*, *121*(4), 1511–1531. https://doi.org/10.1002/2015JD023718

Vahmani, P., & Jones, A. D. (2017). Water conservation benefits of urban heat mitigation. *Nature Communications*, *8*(1), 1072. https://doi.org/10.1038/s41467-017-01346-1

Vahmani, P., Jones, A. D., & Patricola-DiRosario, C. M. (2019). Interacting implications of climate change, population dynamics, and urban heat mitigation for future exposure to heat extremes. *Environmental Research Letters*, *14*(8), 084051. https://doi.org/10.1088/1748-9326/ab28b0

Yi, S., Li, X., Liu, Y., Dong, X., & Tu, W. (2025). A sub-meter resolution urban surface albedo dataset for 34 U.S. cities based on deep learning. *Scientific Data*, *12*(1), 789. https://doi.org/10.1038/s41597-025-05109-2

There is a section break above, please do not delete it.